

See discussions, stats, and author profiles for this publication at: <https://www.researchgate.net/publication/231654506>

Conditions of Simultaneous Growth and Separation of Single- and Multiwalled Carbon Nanotubes

ARTICLE in THE JOURNAL OF PHYSICAL CHEMISTRY C · DECEMBER 2009

Impact Factor: 4.77 · DOI: 10.1021/jp909279g

CITATIONS

11

READS

41

7 AUTHORS, INCLUDING:



[Vyacheslav Khavrus](#)
Technische Universität Dresden
44 PUBLICATIONS 385 CITATIONS

[SEE PROFILE](#)



[E.M.M. Ibrahim](#)
Sohag University
34 PUBLICATIONS 326 CITATIONS

[SEE PROFILE](#)



[A. Leonhardt](#)
Leibniz Institute for Solid State and Materia...
185 PUBLICATIONS 3,323 CITATIONS

[SEE PROFILE](#)



[Bernd Büchner](#)
Leibniz Institute for Solid State and Materia...
1,043 PUBLICATIONS 15,155 CITATIONS

[SEE PROFILE](#)

Conditions of Simultaneous Growth and Separation of Single- and Multiwalled Carbon Nanotubes

Vyacheslav O. Khavrus,*^{†,‡} E. M. M. Ibrahim,^{†,§} Albrecht Leonhardt,[†] Silke Hampel,[†] Steffen Oswald,[†] Christine Täschner,[†] and Bernd Büchner[†]

Leibniz Institute of Solid State and Material Research Dresden, P.O. Box 270016, D-01171 Dresden, Germany, L. V. Pisarzhevsky Institute of Physical Chemistry, National Academy of Sciences of Ukraine, pr. Nauky 31, Kyiv 03028, Ukraine, and Department of Physics, Faculty of Science, Sohag University, Sohag, 82524, Egypt

Received: September 27, 2009; Revised Manuscript Received: November 13, 2009

In this paper, we report conditions of the simultaneous, but separated, deposition of single- and multiwalled carbon nanotubes (SWCNTs, MWCNTs) in one and the same CVD process by a thermal decomposition of acetonitrile and ferrocene at different ratios. We have found an effective separation between SWCNTs and MWCNTs inside the reactor. The MWCNTs are formed on the hot reactor wall, whereas the SWCNTs are spontaneously originated in the gas phase. By means of an argon gas flow, they are transported through the quartz tube reactor and collected on a cooling finger. The morphology and purity of the pristine material are dependent on the amount of evaporated acetonitrile and C/Fe ratio in the gas phase. The reasons for the observed phenomena are discussed.

1. Introduction

Single- and multiwalled carbon nanotubes (SWCNTs and MWCNTs) are well-known nanostructures with excellent mechanical, electronic, and thermal properties.^{1–5} It is today still a grand challenge to prepare bulk material that contains pure single- or multiwalled CNTs with a defined structure, diameter, and length.^{3,6}

For the synthesis of CNTs, several methods, such as arc discharge, laser ablation, and catalytic chemical vapor deposition (CCVD), are known.³ CCVD has proved to be the most convenient way to produce all kinds of carbon nanotubes.⁴ The main difficulty in this process is the preparation of uniform catalyst particles because the diameter distribution of the deposited CNTs and their type (SWCNTs or MWCNTs) are reflected directly by the diameter distribution of the catalyst nanoparticles.^{7–9} Nonuniform particles lead mainly to a mixture of MWCNTs with different inner and outer diameters. However, although significant progress has been made in the synthesis of uniform nanoparticle catalysts for growth of desired CNTs, it is still a great challenge to make nanotubes with a good control of their diameter. We report on the results that come close to the goal of diameter control and the selection of CNT types.

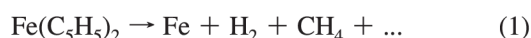
Biró et al. found that it is possible to synthesize a mixture of SWCNTs and MWCNTs simultaneously.¹⁰ Villalpando-Paez et al. mentioned that multiwalled carbon nanotube material was obtained during aerosol-assisted CCVD inside the furnace region (hot zone), and soon thereafter, SWNT strands were collected outside the reaction zone in the cooler region.¹¹ Mathur et al. have shown that, using the electric arc method, SWCNT bundles and MWCNTs can be deposited separately.¹² Bachmatiuk et al. presented results that indicate that low carbon feed rates of

ethanol as carbon source yielded double-walled CNTs and SWCNTs, whereas higher carbon feed rates yielded MWCNTs. However, in this paper, there is no indication for a possible separation of the different types of CNTs.¹³ A similar idea was demonstrated by Zhang et al. who found that a small ethylene flow or a large hydrogen flow tends to synthesize CNTs with small diameters and few wall numbers.¹⁴

Here, we report the spatially separated coproduction of single- and multiwalled CNTs using a high-pressure CCVD process based on some of the before mentioned results that include the possibility of their simultaneous synthesis^{10–12} and the control of their properties by the concentration of the initial feedstock.^{13,14} We discuss the importance of different mechanisms of SWCNT and MWCNT formation and their preferential growth “on demand” using the same device, depending on the C/Fe ratio in the initial feedstock.

2. Experimental Section

For the CNT synthesis, ferrocene ($\text{Fe}(\text{C}_5\text{H}_5)_2$) as the volatile catalyst precursor and acetonitrile as an additional carbon source are used. Their decomposition is dependent on the temperature as well as the pressure in the reactor.^{15–18}



* To whom correspondence should be addressed. Tel: (+49) 351 4659761. Fax: (+49) 351 4659313. E-mail: V.Khavrus@ifw-dresden.de (V.O.K.), vhavrus@yahoo.com (V.O.K.).

[†] Leibniz Institute of Solid State and Material Research Dresden.

[‡] L. V. Pisarzhevsky Institute of Physical Chemistry, National Academy of Sciences of Ukraine.

[§] Sohag University.

As can be expected from the principle of Le Chatelier, raising the pressure suppresses reactions 1–4; in other words, the deposition rate of CNTs will decrease with increasing pressure. On the other hand, the total yield of deposited carbon can be

TABLE 1: Concentration of Acetonitrile in the Reaction Zone Depending on the Construction of the Boat for Its Evaporation. The Rate of the Ferrocene Sublimation Was Constant in All Experiments (15 mg/h)

boat for acetonitrile evaporation	evaporation rate of acetonitrile [g/h]	average concentration of carbon atoms in reaction zone [mol/sccm]	C/Fe atomic ratio
No acetonitrile	0 (N)	$8.7 \cdot 10^{-9}$	10
	0.14 (L)	$8.3 \cdot 10^{-8}$	52
	0.75 (M)	$4.0 \cdot 10^{-7}$	237
	1.63 (H)	$8.7 \cdot 10^{-7}$	502

increased by elevated pressure as a result of increased molar concentrations of the precursors. Recently, we have shown that the high-pressure thermal decomposition of pure ferrocene in an argon flow, described by reaction 1, is suitable for the synthesis of SWCNTs.¹⁹ In such a process, the yield of nanotubes is limited by the low fixed ratio between carbon and iron atoms in the reaction mixture (10:1). To test a possibility of improving the yield of SWCNTs by increasing the ratio between carbon and iron atoms, we used acetonitrile, which is a promising precursor for the high-yield synthesis of N-doped MWCNTs.²⁰

The synthesis of carbon nanostructures was performed by a high-pressure catalytic chemical vapor deposition (HiPCVD) process and was described in details elsewhere.^{19,21} As mentioned above, the used precursors were ferrocene and acetonitrile. For both precursors, two separate evaporation boats (maintained at 95 °C) were installed outside the high-pressure reactor. To vary the concentration of acetonitrile in the gas phase, three different kinds of boats with different evaporation rates can be chosen. Sketches of the used boats together with the rate of acetonitrile evaporation are presented in Table 1. During the experiment, the evaporation rate of ferrocene was fixed to 0.015 g/h, whereas the three different evaporation boats of acetonitrile generated the following rates: 0.14, 0.75, and 1.63 g/h (see Table 1). These rates corresponded to experimental conditions denoted as L (low), M (moderate), and H (high), respectively. The sample synthesized from pure ferrocene was denoted as N (no acetonitrile). As transport gas, we used argon (700 sccm). A second separate gas pipeline existed for the additional dilution of the reaction gas before the reactor injection (700 sccm). The reactor gas was injected continuously by means of a copper nozzle into the reactor volume. Consequently, the precursors were pyrolyzed in the hot zone of the high-pressure reactor. A cooling finger (water cooling) was positioned in the center of the reactor tube behind the hot zone for the collecting of nanotubes. For all experiments, the growth temperature and the growth pressure in the reaction zone (hot zone) were 900 °C and 6 bar, respectively; the usual reaction time was 1 h. The temperature of the area close to the surface of the cooling finger (cold zone) did not exceed 300 °C. Although the yield of the material (which is collected in the cold zone and typically a few milligrams) can be increased by increasing the reaction time, the total material yield could not be determined precisely. This was due to the fact that some portion of it was carried away to the exhaust along with the gas stream. Selection of growth temperature was based on the results of our previous

experiments in aerosol-assisted CVD²⁰ where we have shown a linear correlation between the tube length and the substrate temperature in the range of 800–900 °C.

After the experiment, the deposited material was investigated by different methods.

A small amount of the product was scratched from the cooling finger or the wall of the quartz tube in the hot zone of the reactor and positioned on a copper grid for SEM (FEI NOVA NANOSEM-200 with an accelerating voltage of ~15 kV) and TEM (FEI Tecnai F 30) investigations.

Samples for the measurements of Raman spectra were prepared as follows. Pristine carbon material was suspended in acetone by sonication for several minutes. A few drops of this suspension was positioned onto aluminum foil. After drying in air, a black film was obtained. Raman spectra were recorded at room temperature using a Raman spectrometer (Fourier transform Raman spectroscopy (FTRS) with a Bruker FT RFS 100/s) with a resolution of 1 cm⁻¹ using argon laser excitation with $\lambda = 1064$ nm (1.17 eV) and a power equal to 100 mW. The Raman spectra are presented “as is” without additional rescaling.

X-ray photoelectron spectroscopy (a PHI 5600 CI (Physical Electronics) system with a hemispheric energy analyzer) was used to examine the stoichiometry of the carbon and nitrogen atoms and the intensity of the types of carbon–nitrogen bonding. Monochromatic Al K α X-ray radiation was used for excitation of the photoelectrons.

3. Results and Discussion

The HiPCVD process results in the formation of a flexible weblike deposit on the cooling finger and a firm black carpet on the surface of the quartz tube in the hot zone of the reactor. We find that the composition of the deposited material in both cases is strongly dependent on the C/Fe ratio that is provided by the controlled addition of acetonitrile (see Table 1). Figure 1 presents SEM images of carbon nanostructures deposited in the cold (left-hand) and the hot (right-hand set of figures) zones, corresponding to Table 1. Figure 1a shows a sample morphology that contains a large amount of carbon-coated Fe particles in mixture with CNTs bundles. In the corresponding hot zone, we observe no deposition of any carbonaceous material. The addition of a small amount of acetonitrile (L ratio) causes the production of flexible tubular structures in the cold zone of the reactor; Figure 1b shows their corresponding image. The CNTs possess a length up to a few micrometers. The weblike structure contains also spherical particles with a diameter of up to 100 nm. A further increase of the C/Fe ratio to M and H, respectively, gives a gradual increase of the amorphous carbon content together with tubular structures in the cold zone (see Figure 1d,f). Figure 1f shows that a mixture of nanotube bundles with carbon flakes can be obtained with a high supply of acetonitrile (experimental condition H). The yield of the material collected in the cold zone increases gradually with increasing C/Fe ratio; however, at conditions H, we observe the lowest content of SWCNTs in this material.

The right-hand set of SEM micrographs in Figure 1 displays the properties of the carbon deposit collected from the surface of the quartz tube for increased acetonitrile supply during different experiments. Figure 1c shows the morphology of the material from experiment L. The SEM image shows carbon-coated iron particles with a maximum diameter of about 50 nm. The results for the ratio M are presented in Figure 1e. Only curved tubular structures with a maximum diameter of about 500 nm and a length of not more than a few micrometers are

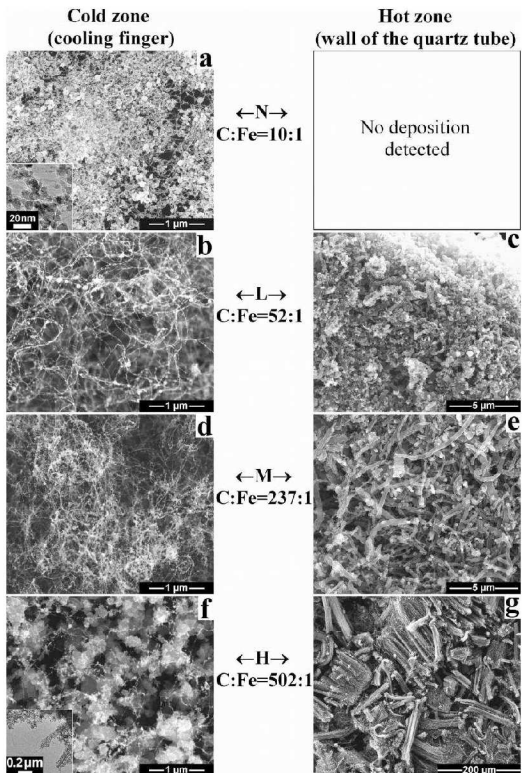


Figure 1. SEM images of carbon nanostructures collected in the cold zone (a, b, d, f) and the hot zone (c, e, g) with pure ferrocene (a) and a different supply of acetonitrile in experiments L (b, c), M (d, e), and H (f, g). Insertions of HRTEM images in (a) and (f) show iron particles and amorphous carbon, respectively.

observed for these conditions. A further increase of the acetonitrile concentration (ratio H) results in the growth of aligned nanotubes with a length of up to a few hundred micrometers on the surface of the quartz tube. Figure 1g shows the morphology of the scratched material. In contradiction to the flexible material deposited in the cold zone, the material was always tightly fixed on the surface of the quartz tube. We observed a maximal yield of carbonaceous material at the ratio H in comparison with conditions L and M.

HRTEM investigations revealed detailed information about the internal structure of the material, as presented in Figure 2. The left-hand set of images shows again the material deposited in the cold zone, whereas the right-hand set of images presents the internal structure of the material scratched from the hot zone for different C/Fe ratios. All left-hand samples show material containing bundles of single-walled carbon nanotubes in mixture with carbon-coated iron particles and amorphous carbon. It is hard to conclude their ratio using the presented scale, but with lower magnification, we observed results that are similar to the ones presented in Figure 1. In all cases, we observed a nearly uniform diameter of SWCNTs that ranges between 0.7 and 0.9 nm. The minimal observed size of the iron particles (Figure 2b) on the surface of the SWCNTs is approximately 1 nm.

The right-hand set of HRTEM micrographs shows the samples for increased acetonitrile supply (Figure 2c,e,g). The results are in agreement with the observations made with the SEM (see Figure 1c,e for ratios L and M, respectively). Figure 2g shows that the long carbon nanotubes (ratio H) have a *bamboo-like* structure; their outer diameter ranges from 60 to 200 nm. Commonly, such bamboo-like structures were found for CNTs prepared by acetonitrile or other nitrogen-containing compounds.^{20,22–27}

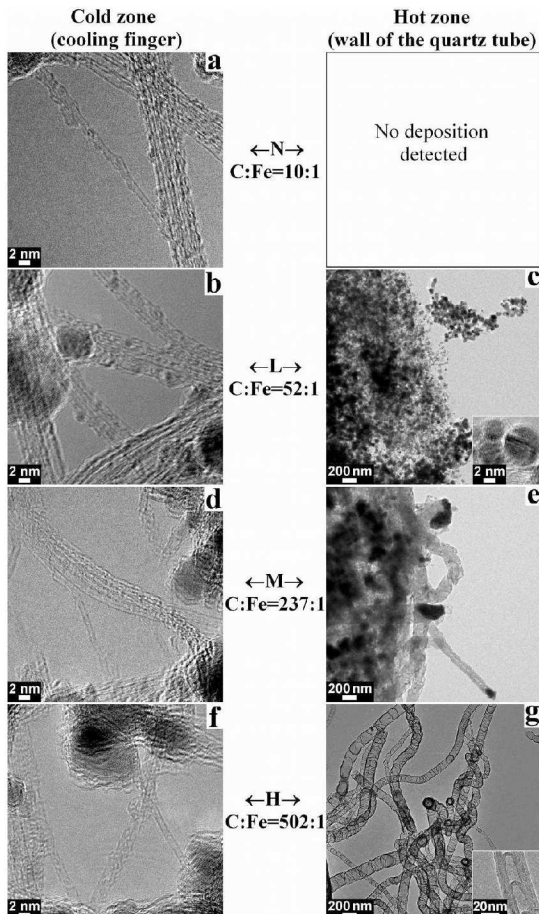


Figure 2. HRTEM images of carbon nanostructures collected in the cold zone (a, b, d, f) and the hot zone (c, e, g) with pure ferrocene (a) and a different supply of acetonitrile in experiments L (b, c), M (d, e), and H (f, g). Insertions of images in (c) and (g) show iron particles and bamboo-like structure of MWCNTs, respectively.

SEM and TEM present us with the results of local investigations. Raman spectroscopy has been shown to be a useful tool to detect the presence of SWCNTs and MWCNTs in the bulk. Figure 3a presents the Raman spectra of carbon nanotube samples from the cold zone and at different C/Fe ratios (N, L, M, H). The well-known radial breathing mode (RBM), disorder-induced mode (D band), and tangential mode (G band) are observed. Their positions are independent of the experimental conditions, whereas the intensities of the bands are strongly dependent on them. A strong RBM peak and multicomponent G band features indicate that the material contains SWCNTs.^{28,29} Samples synthesized using pure ferrocene (N) and at conditions denoted as L and M have strong signals for fundamental modes, whereas sample H (see also Figure 1f) displays a weak signal that has only a poor and noisy RBM mode. This indicates a low content of SWCNTs in the analyzed sample.

The position of the RBM is very sensitive to the chirality of SWCNTs, which are in resonance with the wavelength of the laser beam.^{28–30} The strongest RBM peak is situated for all samples at 266 cm^{-1} , and two other weakly resolved peaks are located at ~ 164 and $\sim 118\text{ cm}^{-1}$, respectively (Figure 3a). The observed RBM modes are in relatively good agreement with the expected modes from the Kataura plot.³⁰ Transition at 266 cm^{-1} shows deviations to the Kataura plot. This deviation was also observed experimentally by Borowiak-Palen et al.³¹ and is well-understood in terms of the strong excitonic nature of the lowest electronic transitions in SWCNTs.³² The diameter of the detectable SWCNTs scales inversely to the position of the RBM

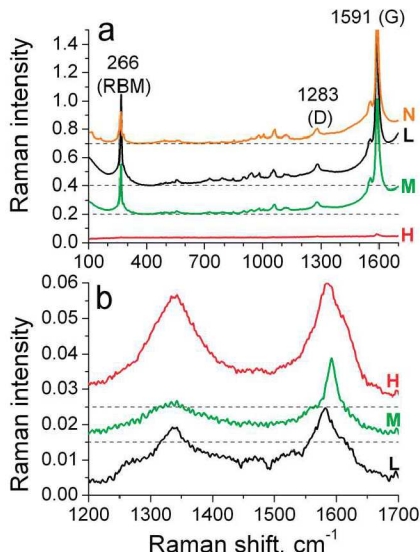


Figure 3. Raman spectra for the carbon material synthesized with different C/Fe atomic ratios and collected from the cooling finger (a) and from the wall of the quartz tube in the hot zone (b). The spectra are shifted for better viewing in the vertical direction without scaling; the corresponding baselines are presented by dashed lines.

peak and can be determined using the expression, d (nm) = $248/\nu$, where ν = RBM frequency (cm^{-1}).³³ Corresponding calculations using the detected RBM peaks give the diameters of SWCNTs observed by Raman spectroscopy with a laser wavelength of 1064 nm to be 0.93, 1.51, and 2.10 nm, respectively.

Figure 3b represents the Raman spectra of the carbon material collected from the hot wall. The intensities of the fundamental lines of the spectra are very low compared to those presented in Figure 3a. The absence of RBM peaks in the spectrum (the RBM region is not shown in Figure 3b) indicates that this material does not contain SWCNTs.²⁹ The presented Raman spectrum is similar to typical spectra of nitrogen-doped MWCNTs^{34,35} that demonstrate wide D and G bands with the value $I_G/I_D \approx 1$. Finally, the comparison of spectra in Figure 3a,b confirms the separated deposition of single- and multiwalled carbon nanotubes in the cold and hot zone of the reactor, respectively.

Therefore, Raman spectra show that material collected in the cold and hot zones at different C/Fe ratios has different morphologies. To compare properties of the most pure SWCNTs and MWCNTs synthesized at conditions L and H, respectively, we used X-ray photoelectron spectroscopy, which is a perfect tool for nondestructive surface chemical analysis. Figure 4 shows XPS of N 1s, C 1s, O 1s, and Fe 2p_{3/2} core levels for SWCNTs (experiment L, black line) and MWCNTs (experiment H, red line) prepared by HiPCVD. The XPS of the N 1s core level for the SWCNT sample (black line in Figure 4a) shows a strong peak at 399.5 eV, which is situated between regions belonging to pyridine-like and graphite-like nitrogen with expected peaks at ~ 399 eV and 400–402 eV, respectively.^{27,36} The peak for MWCNTs is shifted to 401.1 eV, which corresponds to pure graphite-like nitrogen. The observed difference in N incorporation for SWCNTs and MWCNTs is caused by their different formation mechanisms, although the chemical composition of the gas phase in the hot zone is the same for both kinds of CNTs. The XPS of the C 1s core level confirms additionally the presence of nitrogen in the graphite layer because the C 1s peak is stretched to higher binding energies compared with undoped carbon.³⁶ Figure 4b shows an example of this phe-

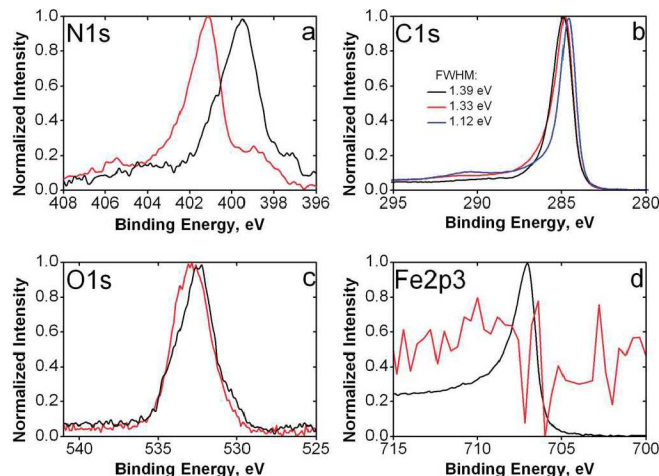


Figure 4. XPS of N 1s (a), C 1s (b), O 1s (c), and Fe 2p_{3/2} (d) core levels for SWCNTs (experiment L, black line) and MWCNTs (experiment H, red line) prepared in HiPCVD. The blue line in (b) shows the spectrum for a N-free sample of SWCNTs synthesized by laser ablation with a more narrow carbon peak compared with that of the analyzed samples.

TABLE 2: Concentration of Chemical Elements in As-Synthesized Samples, Measured by XPS

sample	concentration, atom %			
	C	N	O	Fe
SWCNTs (Figures 1b and 2b)	88.7	2.5	4.2	4.6
MWCNTs (Figures 1g and 2g)	93.0	3.1	3.9	0.0

nomenon; for comparison, the C 1s peak for nitrogen-free SWCNTs prepared by laser ablation is presented. It is possible that, because some carbon atoms are closer to a nitrogen atom in the graphite matrix than others, some carbon atoms will inherently have a higher C 1s binding energy. The C 1s peak has been shown to grow wider as more nitrogen is added to the graphite.³⁷ Figure 4b displays also a broadening of the C 1s peak for N-doped and N-free samples. Figure 4c shows that no significant difference for O 1s peaks is observed for SWCNT and MWCNT samples. However, a corresponding comparison of Fe 2p_{3/2} core levels for SWCNTs and MWCNTs presented in Figure 4d shows that the SWCNTs display a well-defined peak, but the corresponding one for MWCNTs is on the level of the noise. The last result can be easily understood if one takes into account that XPS is a surface method of chemical analysis that shows the chemical composition of the surface layer with a depth of about a few nanometers. It is obvious that iron particles encapsulated inside of multiwalled carbon nanotubes with a thick carbon layer cannot be detected by XPS, whereas such detection is possible for iron particles covered by only a few carbon shells in the SWCNT bundles.

Information about the element composition on the surface of the SWCNTs and MWCNTs determined by XPS analyses is presented in Table 2. The concentration of chemical elements on the surface is estimated from the ratio of the peak areas belonging to the element and the sum of the peak areas of all elements, taking into account standard single-element sensitivity factors. The analysis of the presented data shows that both samples have nitrogen as a building element of the walls of the nanotubes; the corresponding concentration varies in the range of 2.5–3.0 atom %. Therefore, the synthesized SWCNTs and MWCNTs can be attributed to nitrogen-doped carbon nanotubes. The concentration of oxygen in the sample is about 3.9–4.2 atom % primarily as a result of a secondary oxidation of the

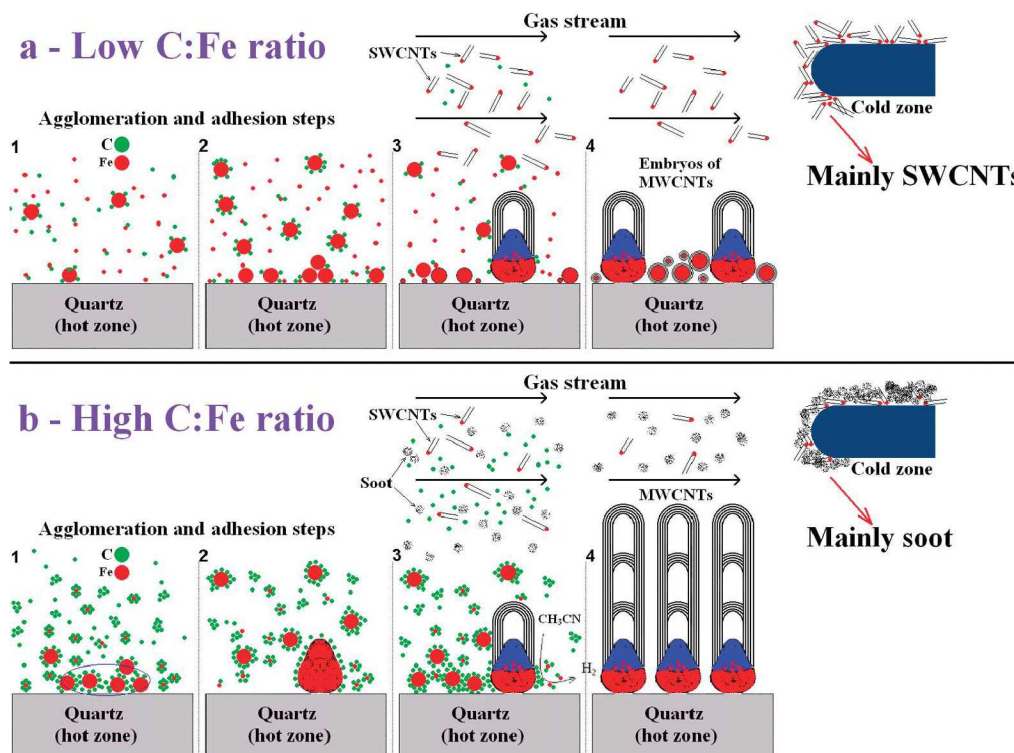


Figure 5. Proposed model for the simultaneous growth and separation of single- and multiwalled nanotubes at low (a) and high (b) C/Fe ratios. Formation of the catalyst particle (early stages 1 and 2) is dependent on the C/Fe ratio, which has also an influence on the material composition at stages 3 and 4. MWCNTs form on the quartz tube wall (support), in agreement with the base-growth mechanism, whereas SWCNTs spontaneously appear in the gas phase.

pristine material during the manipulation in air. The analysis confirms a very low concentration of iron in the surface-near region of MWCNTs, whereas SWCNTs contain iron with a concentration that exceeds 4 atom %.

The separated deposition of single- and multiwalled CNTs can be explained by the different formation mechanisms of both tube kinds (see Figure 5). By the injection of the cold reaction gas ($T \leq 100$ °C as a result of the watercooling system) into the reactor, both ferrocene and acetonitrile are spontaneously decomposed, corresponding to reactions 1–4. During these reactions, iron particles with different diameters can be primarily formed in the gas phase. The very small iron particles (~1 nm) are the origin for the spontaneous growth of single-walled carbon nanotubes. These lightweight SWCNTs are carried away with the gas flow and form a deposit on the cooling finger. On the other hand, the heavy particles hit on the hot quartz wall before CNTs are growing (see stages 1 and 2 in Figure 5a,b). Apparently, the intensity of the agglomeration of iron atoms generated from ferrocene with its constant concentration in the gas phase is dependent on the concentration of carbon species and carbonaceous products generated from them. Increasing concentration of soot and amorphous carbon in the gas phase provides a better condition for adsorption of tiny iron particles on their surface, followed by subsequent agglomeration and deposition on the wall of the device. After that, these particles become the origin for the base growth of bamboo-like MWCNTs, as described earlier (see stages 3 and 4 in Figure 5b).^{18,22,38} Subsequently, the periodic growth of bamboo-like MWCNTs is possible with a permanent and sufficient supply of carbon source for their formation.^{22,38} The results of experiments at ratio L (Figures 1c and 2c) show that the growth of MWCNTs is suppressed; instead, mainly embryos of MWCNTs and carbon-coated iron particles are formed (see Figure 5a). The formation of thick walls of MWCNTs requires a larger amount of carbon.

Obviously, the increase of carbon concentration causes an improved yield and quality of the formed MWCNTs (see the results at the ratios M and H) (see Figure 5b). However, independent of the concentration of carbon, the MWCNTs always stay fixed to the surface of the quartz tube and cannot reach the cold zone of the reactor. As a result, a separation of single- and multiwalled CNTs takes place in the reactor.

We believe that the purity of the produced SWCNTs is strongly dependent on the C/Fe ratio in the gas phase. Earlier, we have shown that the high-pressure thermal decomposition of pure ferrocene gives SWCNTs.¹⁹ The low C/Fe ratio leads to a low yield of SWCNTs. It can be improved by increasing the C/Fe ratio with the addition of an organic compound that is suitable for the growth of CNTs. Indeed, a gaseous feedstock with $C/Fe = 52$ (see Table 1) gives SWCNTs in the cold zone but also mainly carbon-coated iron particles with embryos of MWCNTs in the hot zone of the reactor (see Figure 5a). A moderate supply of carbon in the initial feedstock with a C/Fe ratio of 237 allows both single- and multiwalled CNTs to be synthesized. However, an excess of carbon (ratio of $C/Fe > 500$) causes mainly the active pyrolysis of CH_3CN without significant catalytic action of the iron particles for growth of SWCNTs. As a result, the formation of soot and amorphous carbon in the gas phase coupled with the active growth of MWCNTs in the hot zone is preferred (see Figure 5b).

Finally, we believe that the described idea of variation of the C/catalyst ratio can help to develop a high-yield device that is capable for separate synthesis of SWCNTs or MWCNTs “on demand” using a volatile catalyst compound and hydrocarbon with their molar ratio suitable for desired product(s). The main point for the proper selection couple catalyst–hydrocarbon is the base-growth mechanism of MWCNTs on a fixed support and spontaneous formation of SWCNTs in the gas phase.

4. Conclusions

We have shown that the separate and simultaneous synthesis of SWCNTs and MWCNTs in one and the same reactor, dependent on the atomic ratio of carbon to iron in the initial ferrocene–acetonitrile feedstock, can be realized. As a result of different formation processes, the SWCNTs are always deposited from the gas stream in the cold zone of the reactor, whereas the MWCNTs are formed on the quartz tube wall by the base-growth mechanism in the hot zone. A low C/Fe ratio gives mainly SWCNTs and embryos of MWCNTs, whereas a high C/Fe ratio facilitates deposition of long well-aligned MWCNTs and SWCNTs in mixture with carbon-coated iron particles and amorphous carbon. A moderate C/Fe atomic ratio of ~ 240 yields the optimal results with a relatively high quality and yield of SWCNTs and MWCNTs in separate deposits. The complete separation and properties of both kinds of nanotubes is shown using SEM, HRTEM, XPS, and Raman investigations. The synthesis process can be optimized in the future by using other hydrocarbons suitable for the synthesis of CNTs.

Acknowledgment. The authors are grateful to Sieglinde Pichl and Gesine Kreutzer for help with SEM and HRTEM measurements. The authors acknowledge the assistance of Franziska Wolny for help in preparation of the manuscript. V.O.K. gratefully acknowledges financial support from the Leibniz Institute for Solid State and Materials Research Dresden, the Saxon Ministry of Science and the Fine Arts, and Deutsche Forschungsgemeinschaft. E.M.M.I. thanks the Leibniz Institute for Solid State and Materials Research Dresden and acknowledges the Egyptian Ministry of Higher Education and Scientific Research for financial support through a postdoctoral fellowship.

References and Notes

- (1) Baughman, R. H.; Zakhidov, A. A.; de Heer, W. A. *Science* **2002**, 297, 787.
- (2) Robertson, J. *Mater. Today* **2004**, 7, 46.
- (3) Ando, Y.; Zhao, X.; Sugai, T.; Kumar, M. *Mater. Today* **2004**, 7, 22.
- (4) Melechko, A. V.; Merkulov, V. I.; McKnight, T. E.; Guillorn, M. A.; Klein, K. L.; Lowndes, D. H.; Simpson, M. L. *J. Appl. Phys.* **2005**, 97, 041301.
- (5) Avouris, P.; Chen, Z.; Perebeinos, V. *Nat. Nanotechnol.* **2007**, 2, 605.
- (6) Suárez, B.; Simonet, B. M.; Cárdenas, S.; Valcárcel, M. *J. Chromatogr., A* **2006**, 1128, 282.
- (7) Dupuis, A.-C. *Prog. Mater. Sci.* **2005**, 50, 929.
- (8) Bartsch, K.; Arnold, B.; Kaltoven, R.; Täschner, C.; Thomas, J.; Leonhardt, A. *Carbon* **2007**, 45, 543.
- (9) Fu, Q.; Huang, S.; Liu, J. *J. Phys. Chem. B* **2004**, 108, 6124.
- (10) Biró, L. P.; Horváth, Z. E.; Koós, A. A.; Osváth, Z.; Vértesy, Z.; Darabont, A.; Kertész, K.; Neamtu, C.; Sárközi, Zs.; Tapasztó, L. *J. Optoelectron. Adv. Mater.* **2003**, 5, 661.
- (11) Villalpando-Paez, F.; Zamudio, A.; Elias, A. L.; Son, H.; Barros, E. B.; Chou, S. G.; Kim, Y. A.; Muramatsu, H.; Hayashi, T.; Kong, J.; Terrones, H.; Dresselhaus, G.; Endo, M.; Terrones, M.; Dresselhaus, M. S. *Chem. Phys. Lett.* **2006**, 424, 345.
- (12) Mathur, R. B.; Seth, S.; Lal, C.; Rao, R.; Singh, B. P.; Dhami, T. L.; Rao, A. M. *Carbon* **2007**, 45, 132.
- (13) Bachmatiuk, A.; Borowiak-Palen, E.; Kalenczuk, R. *J. Nanotechnology* **2008**, 19, 365605.
- (14) Zhang, H.; Cao, G.; Wang, Z.; Yang, Y.; Shi, Z.; Gu, Z. *J. Phys. Chem. C* **2008**, 112, 12706.
- (15) Dyagileva, L. M.; Marin, V. P.; Tsyananova, E. I.; Razuvayev, G. A. *J. Organomet. Chem.* **1979**, 175, 63.
- (16) Sendt, K.; Ikeda, E.; Bacska, G. B.; Mackie, J. C. *J. Phys. Chem. A* **1999**, 103, 1054.
- (17) Leonhardt, A.; Hampel, S.; Müller, C.; Mönch, I.; Koseva, R.; Ritschel, M.; Elefant, D.; Biedermann, K.; Büchner, B. *Chem. Vap. Deposition* **2006**, 12, 380.
- (18) He, M.; Zhou, S.; Zhang, J.; Liu, Z.; Robinson, C. *J. Phys. Chem. B* **2005**, 109, 9275.
- (19) Barreiro, A.; Hampel, S.; Rümmeli, M. H.; Kramberger, C.; Grüneis, A.; Biedermann, K.; Leonhardt, A.; Gemming, T.; Büchner, B.; Bachtold, A.; Pichler, T. *J. Phys. Chem. B* **2006**, 110, 20973.
- (20) Khavrus, V. O.; Leonhardt, A.; Hampel, S.; Täschner, C.; Müller, C.; Gruner, W.; Oswald, S.; Strizhak, P. E.; Büchner, B. *Carbon* **2007**, 45, 2889.
- (21) El-Gendy, A. A.; Ibrahim, E. M. M.; Khavrus, V. O.; Krupskaya, Y.; Hampel, S.; Leonhardt, A.; Büchner, B.; Klingeler, R. *Carbon* **2009**, 47, 2821.
- (22) Terrones, M.; Benito, A. M.; Manteca-Diego, C.; Hsu, W. K.; Osman, O. I.; Hare, J. P.; Reid, D. G.; Terrones, H.; Cheetham, A. K.; Prassides, K.; Kroto, H. W.; Walton, D. R. M. *Chem. Phys. Lett.* **1996**, 257, 576.
- (23) Nath, M.; Satishkumar, B. C.; Govindaraj, A.; Vinod, C. P.; Rao, C. N. R. *Chem. Phys. Lett.* **2000**, 322, 333.
- (24) Hao, Y.; Qingwen, L.; Jin, Z.; Zhongfan, L. *Chem. Phys. Lett.* **2003**, 380, 347.
- (25) Kudashov, A. G.; Okotrub, A. V.; Bulusheva, L. G.; Asanov, I. P.; Shubin, Yu. V.; Yudanov, N. F.; Yudanova, L. I.; Danilovich, V. S.; Abrosimov, O. G. *J. Phys. Chem. B* **2004**, 108, 9048.
- (26) Amadou, J.; Chizari, K.; Houllé, M.; Janowska, I.; Ersen, O.; Bégin, D.; Pham-Huu, C. *Catal. Today* **2008**, 138, 62.
- (27) Ewels, C. P.; Glerup, M. *J. Nanosci. Nanotechnol.* **2005**, 5, 1345.
- (28) Dresselhaus, M. S.; Dresselhaus, G.; Saito, R.; Jorio, A. *Phys. Rep.* **2005**, 409, 47.
- (29) Dresselhaus, M. S.; Dresselhaus, G.; Jorio, A. *J. Phys. Chem. C* **2007**, 111, 17887.
- (30) Kataura, H.; Kumazawa, Y.; Maniwa, Y.; Umezawa, I.; Suzuki, S.; Ohtsuka, Y.; Achiba, Y. *Synth. Met.* **1999**, 103, 2555.
- (31) Borowiak-Palen, E.; Bachmatiuk, A.; Rümmeli, M. H.; Gemming, T.; Kruszynska, M.; Kalenczuk, R. *J. Physica E* **2008**, 40, 2227.
- (32) Maultzsch, J.; Pomraenke, R.; Reich, S.; Chang, E.; Prezzi, D.; Ruini, A.; Molinari, E.; Strano, M. S.; Thomsen, C.; Lienau, C. *Phys. Rev. B* **2005**, 72, 241402(R).
- (33) Jorio, A.; Saito, R.; Hafner, J. H.; Lieber, C. M.; Hunter, M.; McClure, T.; Dresselhaus, G.; Dresselhaus, M. S. *Phys. Rev. Lett.* **2001**, 86, 1118.
- (34) Maldonado, S.; Morin, S.; Stevenson, K. J. *Carbon* **2006**, 44, 1429.
- (35) Bulusheva, L. G.; Okotrub, A. V.; Kinloch, I. A.; Asanov, I. P.; Kurenya, A. G.; Kudashov, A. G.; Chen, X.; Song, H. *Phys. Status Solidi B* **2008**, 245, 1971.
- (36) Tran, N. H.; Wilson, M. A.; Milev, A. S.; Bartlett, J. R.; Lamb, R. N.; Martin, D.; Kannangara, G. S. K. *Adv. Colloid Interface Sci.* **2009**, 145, 23.
- (37) Matter, P. H.; Zhang, L.; Ozkan, U. S. *J. Catal.* **2006**, 239, 83.
- (38) Kuznetsov, V. L. In *Nanoengineered Nanofibrous Materials*; Guceri, S. I., Gogotsi, Y., Kuznetsov, V., Eds.; NATO Science Series 169 NATO-ASI (PST 979397); Kluwer Academic Book Publishers: Dordrecht, Netherlands, 2004; pp 19–34.

JP909279G